Desalination 458 (2019) 122–135

Contents lists available at ScienceDirect

Desalination

journal homepage: www.elsevier.com/locate/desal

Super-twisting sliding mode control and robust loop shaping design of RO desalination process powered by PV generator

Mohamed Zebbar[a,*], Youcef Messlem[a], Abdelmadjid Gouichiche[a], Mohamed Tadjine[b]

[a] Laboratoire de Génie électrique et des plasmas, Université Ibn Khaldoun, Tiaret, Algeria
[b] Laboratoire de Commande des Processus, Ecole Nationale Polytechnique Alger, Algeria

ARTICLE INFO

Keywords:
Desalination
Reverse osmosis (RO)
Stand-alone photovoltaic (PV) system
Control design
Loop shaping
Super-twisting

ABSTRACT

Reverse osmosis (RO) desalination technique is the most widely used technology for supplying fresh water since it offers many advantages. Developing an accurate control strategy is one of the most challenging jobs in RO desalination plant especially under uncertainties and disturbances conditions to avoid all possible system failures and damages for safe operations. This paper presents an overall architecture of reverse osmosis desalination process supplied by a stand-alone photovoltaic (PV) system. A dynamic modeling of various components of this architecture is developed. A control strategy of the whole system is addressed with a controller for each part. Furthermore, special attention is given here to the robust control design of reverse osmosis (RO) membrane to address large set point changes and capability to reject external disturbances and to cope with parametric uncertainties as variations in feed water salinity. The control block is divided into two loops the first one using the loop shaping design method and the super-twisting sliding mode control is applied for the second loop. Simulation results investigating different scenarios show the efficiency of the proposed scheme.

1. Introduction

Desalination is a process that produces drinkable water, removing most of the salt from a water stream (sea or brackish). Furthermore, It can treat waters of different origins: seawater (whose salt concentration varies between 35 and 49 g/l), brackish water and ground-water (where the salt concentration varies from 1 to 10 g/l) [1,2]. There are several desalination technologies and several ways to classify them; some are more suited to a given environment than others. At present, five techniques are used, grouped into two families: distillation processes and membrane processes. Both operate on the same principle that separates saline water into two streams: the freshwater stream with a low concentration of dissolved salts and the concentrate (brine) stream. Regardless of the technology used, all desalination plants require energy to operate and need a chemical pretreatment unit of raw brackish water (or seawater) and chemical post-treatment of the processed water [3,4]. In recent years, RO membrane desalination has emerged as one of the leading methods for water desalination [5] because it provides attractive advantages compared to other technologies in terms of simplicity in design and operation and low energy consumption. In addition, it is able to produce fresh water at lower cost and better quality because of the development of membranes that can operate efficiently at lower pressures, and the use of energy recovery devices [1,6].

Despite the progress made in desalination technologies the energy needed to operate these plants remains a drawback especially when it is powered by conventional energy sources. However, emissions of greenhouse gases (GHG) which is caused by fossil fuels, and the high cost of its use led to a growing interest in renewable energy sources. Over the last quarter century, renewable energy technologies have certainly evolved technically to the point where they should be now considered as clean energy alternatives to fossil fuels [7,8].

Several types of renewable energy can be used in water desalination, but some are more promising than others in terms of technical and economic feasibility. On the other hand, the choice of suitable alternative energy sources for coupling with desalination plant depends on a number of factors. The local availability of renewable energy resources and the salinity of feed water, plant size, accessibility to the grid and technical infrastructure [9]. In fact, solar energy is the most widely used, accounting for nearly 57% of the market for desalination based on renewable energies [3] where the most popular combination of technologies is the use of photovoltaic energy in conjunction with RO desalination.

Several studies have been made in the literature to process control of RO system but most of this works focused on controlling a linear RO model. We mention, for example in [10,11] an effective closed-loop control strategy for Industrial RO desalination processes used

* Corresponding author.
E-mail address: zebbar.mohamed91@gmail.com (M. Zebbar).

https://doi.org/10.1016/j.desal.2019.02.011
Received 8 January 2018; Received in revised form 4 October 2018; Accepted 18 February 2019

traditional PID controllers has been proposed. In [12] authors synthesize a H ∞ controller to regulate the linear RO system using a linear model around the equilibrium points. In addition to linear control schemes, few papers discuss the nonlinear model control of RO system. In [13] a nonlinear feed-forward/feedback control was implemented on a high recovery RO plant model. In [14] a nonlinear model-based control was designed and implemented in the experimental RO membrane desalination process using geometric control techniques. The drawbacks of these studies are they do not consider the additional necessary components for RO system such as the power supply, the pumping process… etc. From our knowledge, it does not exist any works, which consider the study of the complete system containing a power source, pumping process, and reverse osmosis (RO) membrane, taking account of the control of each element of this chain.

Motivated by the previously mentioned considerations, this work proposes a novel application of the super-twisting sliding mode control strategy for RO system. Furthermore, the RO system is integrated in a complete chain containing solar energy and induction motor associated with a centrifugal pump. The main contribution of this paper consists in using a super-twisting algorithm for the control of reverse osmosis (RO) desalination process. The dynamics of the RO system are modeled based on the use of mass and energy balances [14]. In order to act on the flow rate at the outlet of the membrane, the super-twisting control algorithm can maintain the system operation at the desired bypass flow velocity and retentate flow velocity operating point by manipulating the actuated bypass valve and concentration valve, respectively. This control scheme has been designed to obtain good dynamic performances and ensure robustness under noises and parametric uncertainties.

The paper is organized as follows: Section 2 describes the system configuration. Section 3 is devoted to designing the controller for the RO membrane. Simulation results are discussed and analyzed in Section 4. The conclusions are given in the last part of the paper.

2. System configuration

The main idea behind this configuration is to design and construct an RO water desalination system that could be used for almost any type of source water and could be feasible in term of economic and technical purposes.

To achieve this trade-off, we propose the configuration shown in Fig. 1, this architecture can be decomposed in the following blocks: photovoltaic generator (PVG) with energy management block, a DC/DC boost converter, three-phase DC/AC inverter, induction motor (IM) coupled to the centrifugal pump, and RO membrane module.

The photovoltaic panels are used to generate electricity from incident solar radiation as per the photovoltaic effect to feed an induction motor associated with a centrifugal pump, driven by field oriented control (FOC) strategy, via a boost converter controlled by perturb and observe (P&O) maximum power point tracking (MPPT) technique that will be explained in Section 2.1.1, which allows the system operates at maximum power with varying operating conditions and a three-phase voltage inverter generates a variable frequency output waveform. The mechanical energy is converted into hydraulic energy by the group induction motor-centrifugal pump, which delivers a high-pressure water output for supplying the RO module. Energy management system is added in order to guarantee a continuous power flow under different weather conditions where the main objective is to satisfy the power load needed and ensure an uninterruptible service.

The control scheme is divided into two loops; the first one uses the loop shaping PI controller to regulate the system pressure and the second loop using the super-twisting sliding mode control for the RO membrane unit for the subject to regulate the water at the outlet of the membrane.

In the following section, we will discuss the model of each element shown above (Fig. 1).

2.1. Photovoltaic generator (PVG) model

Several mathematical models are used to describe the operation of the photovoltaic generator. Each model considers a different method of calculation and the number of parameters involved in the characteristic of current-voltage [15–17]. Fig. 2 shows the simplified solar (PV) cell equivalent circuit [18].

The I-V characteristic of this model defined by the following equations [19]:

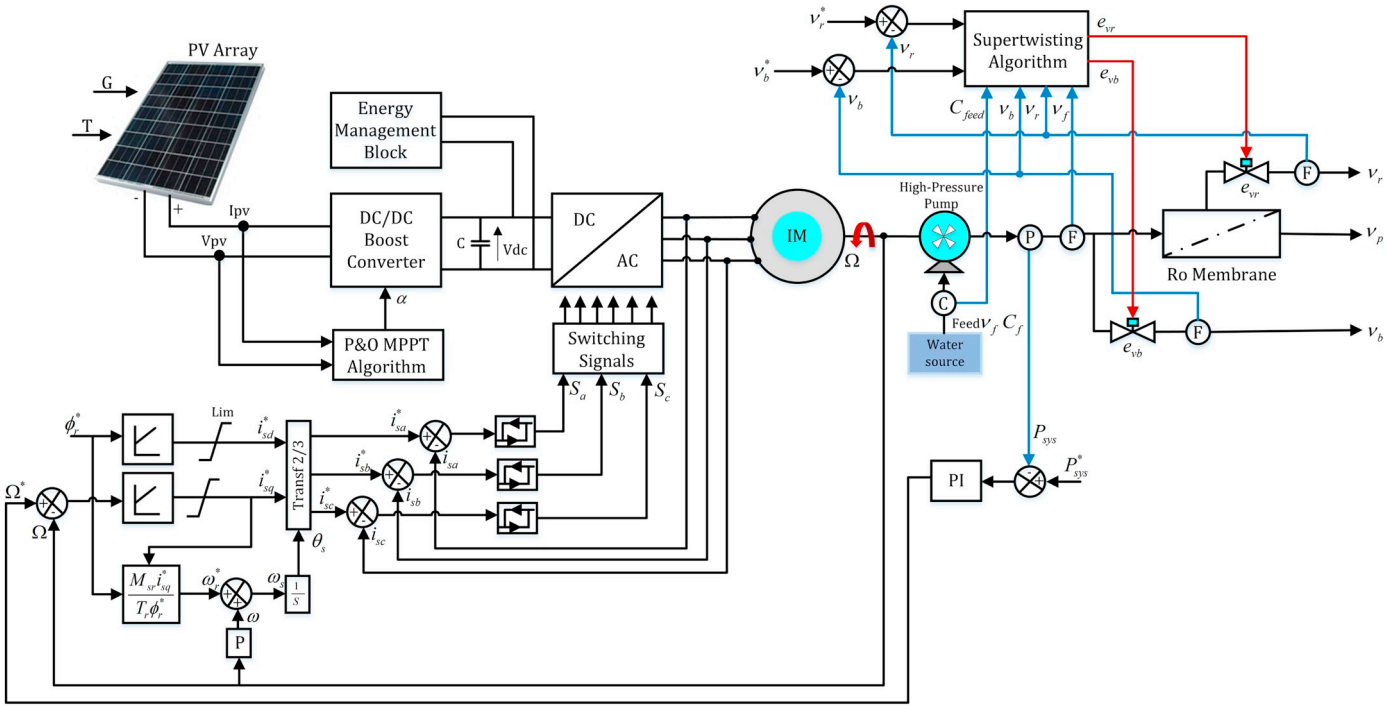

Fig. 1. The proposed RO desalination system.

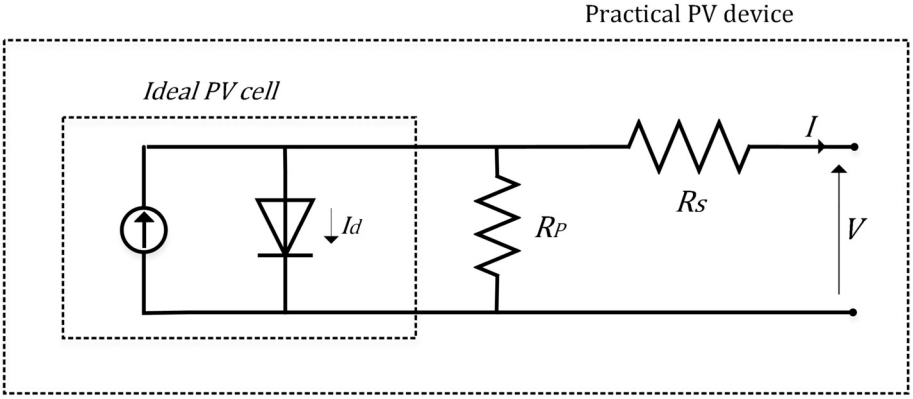

Fig. 2. The equivalent circuit of the solar cell.

$$I = I_{pv} - I_0\left[\exp\left(\frac{V + R_s I}{V_t \alpha}\right) - 1\right] - \frac{V + R_s I}{R_p} \quad (1)$$

With

$$V_t = \frac{N_s kT}{q} \quad (2)$$

where I_{pv} and I_0 are the photovoltaic currents of array and reverse saturation currents of diode respectively. V_t is the thermal voltage of the array with N_s cells connected in series. T is the temperature of the p-n junction, q is the electron charge ($q = 1.60217646 \cdot 10^{-19}$ C), k is the Boltzmann constant ($k = 1.3806503 \cdot 10^{-23}$ J/K), and α is the diode ideality factor, R_s is the equivalent series resistance of the array, R_p is the equivalent shunt resistance.

2.1.1. MPPT controller

Maximum power point trackers (MPPT) is a power electronic device interconnecting a PV power source and a load, which allows the system to operate at maximum power with varying operating conditions. MPPT is made up with a switch-mode DC/DC converter whose duty cycle is adjusted for drawing the correct amount of current and therefore maximizes the system efficiency [20–22].

Several algorithms proposed in the literature where perturb and observe (P&O) is one of the most popular method of tracking maximum power in solar PV [22,23]. Due to its simplicity and effectiveness. The operating voltage of the panel is disturbed by introducing a small perturbation in every iteration then the power is compared before and after perturbation to determine the next disturbance direction. If the power drawn from the PV array increases, the following perturbation will remain in the same direction. Otherwise, if the power decreases, the operating point has moved away from the MPP and therefore the new perturbation must be reversed [24,25]. Fig. 3 shows the flowchart of this algorithm.

2.2. Motor-pump subsystem

Centrifugal pump represents the most commonly employed pump type in various industrial applications [25], among which water treatment and aqueous solutions.

In the reverse osmosis (RO) desalination system, centrifugal pumps designed for variable speed operation are the widely used technology. They can be used to transform the rotation speed of the induction motor into a high-pressure water flow rate. This is due to its simple construction with few moving parts, making it very reliable and robust.

This subsection introduces the mathematical model of the centrifugal pump. This includes the vector control induction motor model driving the pump.

2.2.1. Modeling of the centrifugal pump

The hydrodynamic load torque of the centrifugal pump is proportional to the square of the rotational speed of the motor given by [26]:

$$T_L = \mathrm{A}_p \omega_r^2 \quad (3)$$

With

$$\mathrm{A}_p = \frac{P_n}{\omega_{rn}^3} \quad (4)$$

where A_p is the torque constant, P_n is the nominal power of the induction motor and ω_{rn} is the rotor nominal speed.

The centrifugal pump is described by the lows of similarity, which are given by [26,27]:

$$\begin{cases} Q' = (N'/N)Q \\ H' = (N'/N)^2 H \end{cases} \quad (5)$$

where Q' and Q are respectively the flow rate and the nominal flow rate of the pump, H' and H are respectively its height and total height; N' and N are respectively its speed and nominal speed.

2.2.2. Vector control of IM drive and pump coupling

2.2.2.1. Vector control. In this part of the system, the induction motor (IM) is used to drive the high-pressure pump that supplies the reverse osmosis module with sea or brackish water. In general, IM drive can be based on scalar control (v/f) [28], field-oriented control (FOC) and slip control [29]. Highly efficient IM drive systems can be realized using field oriented control strategies. However, these strategies require rotor speed measurement [30]. This control can be realized by orienting the flux on the d axis, which can be expressed as [31]:

$$\phi_{rd} = \phi_r \text{ and } \phi_{rq} = 0 \quad (6)$$

With field orientation, the dynamic equations of stator current components, rotor flux, and electromagnetic torque are given by [31]:

$$\frac{di_{sd}}{dt} = \frac{1}{\sigma L_s}\left(-\left(R_s + \left(\frac{L_m}{L_r}\right)^2 R_r\right) i_{sd} + \sigma L_s \omega_s i_{sq} + \frac{L_m R_r}{L_r^2}\phi_r + V_{sd}\right) \quad (7)$$

$$\frac{di_{sq}}{dt} = \frac{1}{\sigma L_s}\left(-\sigma L_s \omega_s i_{sd} - \left(R_s + \left(\frac{L_m}{L_r}\right)^2 R_r\right) i_{sq} - \frac{L_m}{L_r}\phi_r \omega_r + V_{sq}\right) \quad (8)$$

$$\frac{d\phi_{rd}}{dt} = \frac{L_m R_r}{L_r} i_{sd} - \frac{R_r}{L_r}\phi_r \quad (9)$$

$$Tem = \frac{pL_m}{Lr} i_{sq} \Phi_r \quad (10)$$

With

$\sigma = 1 - \frac{L_m^2}{L_s L_r}$ is the leakage coefficient.

The induction motor vector control allows us to regulate the flux

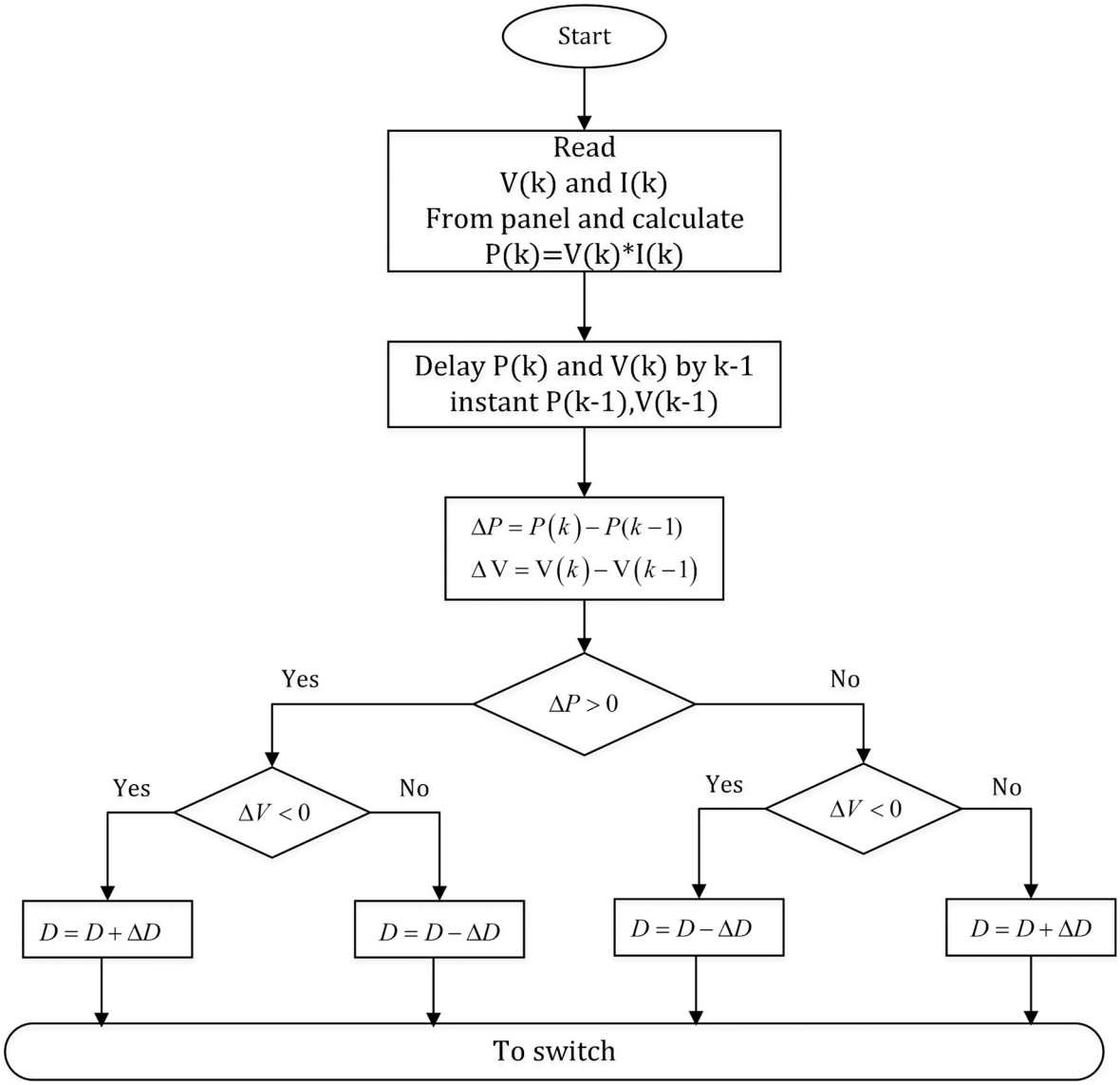

Fig. 3. Flowchart of Perturb and Observe method.

and the torque separately by controlling the corresponding currents i_{sd} and i_{sq}. The desired currents are determined from the PI flux and speed controllers as shown in Fig. 1.

2.2.2.2. Centrifugal pump effect on the IM drive. The mechanical induction motor equation is presented by:

$$J\frac{d\Omega_r}{dt} = T_{em} - f\Omega_r - T_L \tag{11}$$

T_L is unknown load torque generated by the centrifugal pump.

In order to drive the speed Ω_r we need to design a robust controller which maintain the tracking error $(\Omega_r^* - \Omega_r)$ asymptotically stable in the present of unknown load torque due to the centrifugal pump.

2.3. Reverse osmosis (RO) system model

The RO plant consists of a high-pressure pump, two automated valves, a spiral wound membrane unit, with no pretreatment or post-treatment units. As seen in Fig. 4, the feed is water pressurized and sent towards the membrane module by a high-pressure pump. The pressurized stream is split into a bypass stream with velocity v_b and the stream which enters the spiral-wound membrane unit (v_{fr}), where it is separated into a low-salinity product (permeate) stream and concentrate stream with velocity v_r. All of the exit streams discharged at atmospheric pressure [12,32].

The dynamics of the RO system are modeled using the mass and the energy balances. In order to simplify the problem, several assumptions can be invoked [32,33]. The model derivation results in two non-linear ordinary differential equations (ODEs) that can describe the process depicted in Fig. 4 take the following form:

$$\begin{cases} \dfrac{dv_b}{dt} = \dfrac{A_p^2}{A_m K_m V}(v_f - v_b - v_r) + \dfrac{A_p}{\rho V}\Delta\pi - \dfrac{1}{2}\dfrac{A_p e_{vb} v_b^2}{V} \\ \dfrac{dv_r}{dt} = \dfrac{A_p^2}{A_m K_m V}(v_f - v_b - v_r) + \dfrac{A_p}{\rho V}\Delta\pi - \dfrac{1}{2}\dfrac{A_p e_{vr} v_r^2}{V} \end{cases} \tag{12}$$

The bypass velocity (v_b) and retentate velocity (v_r) are the states. V is the total internal volume, A_P is the pipe cross-sectional area, A_m is the membrane area, K_m is the overall mass transfer coefficient of the membrane, ρ is the fluid density, e_{vr} is the retentate valve resistance, e_{vb} is the bypass valve resistance, v_f is the feed velocity, $\Delta\pi$ is the osmotic pressure.

The permeate stream velocity (v_p) and the system pressure (P_{sys}) are respectively defined as:

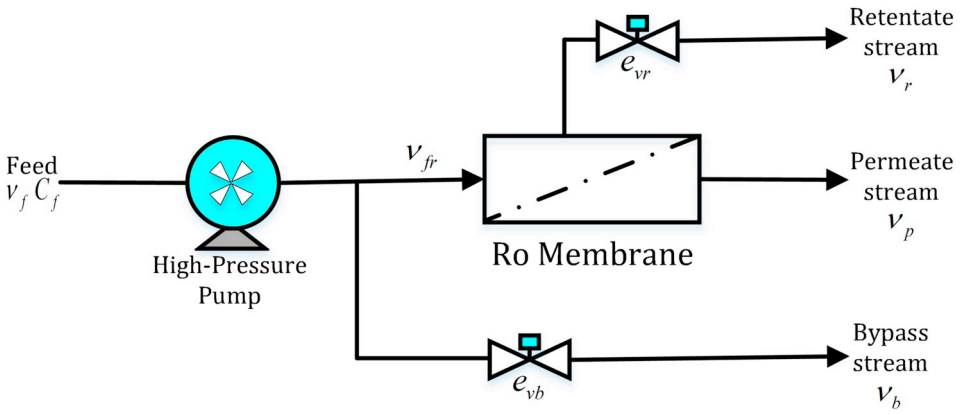

Fig. 4. Schematic of the RO desalination process.

$$v_p = \frac{A_m K_m}{\rho A_p}(P_{sys} - \Delta\pi) \tag{13}$$

$$P_{sys} = \frac{\rho A_p}{A_m K_m}(v_f - v_b - v_r) + \Delta\pi \tag{14}$$

Then the osmotic pressure is further calculated as:

$$\Delta\pi = \delta C_{eff}(T + 273) \tag{15}$$

With

$$C_{eff} = C_{feed}\left(a + (1-a)\left(\frac{(1-R) + R(v_f - v_b)}{v_r}\right)\right) \tag{16}$$

where C_{feed} is the amount of total dissolved solids (TDS) in the feed, δ is a constant relating effective concentration to osmotic pressure, a is an effective concentration-weighting coefficient, R the fractional salt rejection of the membrane, and T process temperature.

Let us consider the system (12) as follows:

$$\begin{cases} \dot{x} = f(x) + g(x)U \\ y = h(x) \end{cases} \tag{17}$$

where

$$\dot{x} = \begin{bmatrix} \dot{x}_1 \\ \dot{x}_2 \end{bmatrix} = \begin{bmatrix} v_b \\ v_r \end{bmatrix},\ U = \begin{bmatrix} u_1 \\ u_2 \end{bmatrix} = \begin{bmatrix} e_{vb} \\ e_{vr} \end{bmatrix},\ y = \begin{bmatrix} v_b \\ v_r \\ P_{sys} \end{bmatrix} \tag{18}$$

And

$$f(x) = \begin{bmatrix} f_1(x) \\ f_2(x) \end{bmatrix} = \begin{bmatrix} \frac{P_{sys}A_p}{\rho V} \\ \frac{P_{sys}A_p}{\rho V} \end{bmatrix} \tag{19}$$

$$g(x) = \begin{bmatrix} g_1(x) \\ g_2(x) \end{bmatrix} = \begin{bmatrix} -\frac{1}{2}\left(\frac{A_p v_b^2}{V}\right) \\ -\frac{1}{2}\left(\frac{A_p v_r^2}{V}\right) \end{bmatrix} \tag{20}$$

Note that, the relative degree of our system is one.

3. Control strategy

Effective operation of RO desalination system requires robust process control strategy and energy optimization along with membrane monitoring which is crucial, for sea or brackish water desalination, to monitor the state of the reverse osmosis (RO) membranes with respect to fouling and mineral salt scaling. In this way, the control algorithm is designed to improve system operation with respect to desired point transitions and with respect to changes in feed water quality in order to allow for safe, reliable RO system operation.

Using the dynamic equations mentioned above, various control techniques can be applied using the valve resistance values as the manipulated inputs (e_{vb}, e_{vr}); the measured outputs are the velocities of the fluid in the bypass lines (v_b), the retentate velocity (v_r) and the system pressure (P_{sys}).

3.1. Control objective

3.1.1. Induction motor speed control loop

For the induction motor the load torque generated by the centrifugal pump (T_r) is unknown for this reason we will design robust PI controller based on the loop shaping that will be explained later in this section.

The block diagram presented in Fig. 5 shows the coupling between

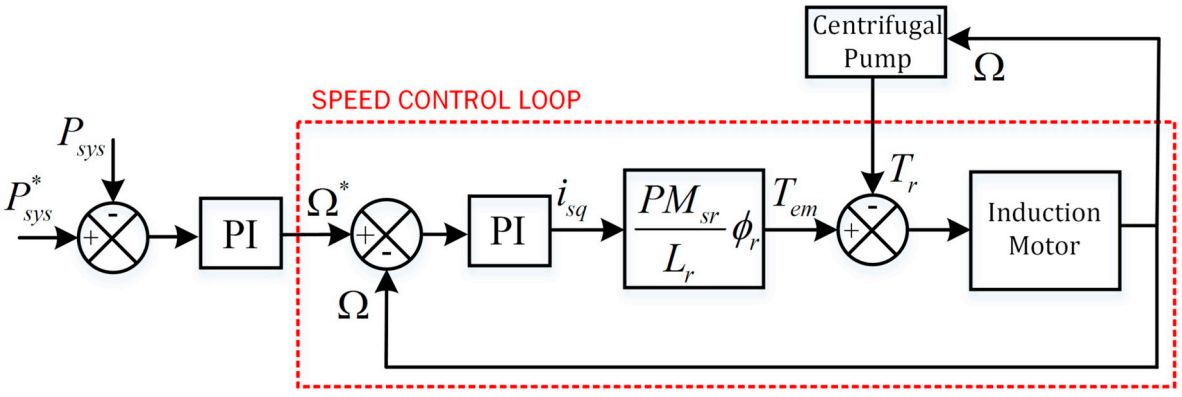

Fig. 5. Speed control loop block diagram.

the induction motor and the centrifugal pump. Besides, the direct relationship between the two loops. Speed control loop and system pressure control loop.

3.1.2. RO system loops

For the RO system, we will focus on the control of two separate loops. The first loop regulates the system pressure by adjusting the variable frequency drive speed (S_{VFD}) directly (effectively changing the feed flow rate) using a robust proportional-integral (PI) feedback controller.

In fact, controlling the system pressure is the key in RO desalination performance. The system presented in this work utilized a constant feed flow rate but used a separate bypass stream with an actuated valve to control the stream velocity of the water feeding to the membrane unit.

The second loop using super-twisting sliding mode control to regulate the bypass and retentate flow velocity (flow rate) where the objective is to stabilize the process at the desired steady-state using the bypass valve and retentate valve (e_{vb}, e_{vr}) respectively as manipulated inputs. Besides, to be able to act on the flow rate at the outlet of the membrane represented by the velocity v_p. Furthermore, the robust controller is synthesized guaranteeing that it can deal with parametric uncertainties such as the feed water variation and disturbances caused by noisy measurements.

Loop 1: the control algorithm of the system pressure (P_{sys}) takes the form:

$$S_{VFD} = K_p(P_{sys}^{sp} - P_{sys}) + K_I \int_0^{tc} (P_{sys}^{sp} - P_{sys})dt \tag{21}$$

where S_{VFD} is the control action applied to the variable frequency drive (VFD) [14] speeds, K_p the proportional gain, and K_I the integral gain.

This controller is designed using "loop shaping design method" (Fig. 6). in order to achieve performance and robustness by ensuring "high" open loop gain at low frequencies and "low" open loop gain at high frequencies [34].

Let G(s) the transfer function of the controlled system, which is computed as follows:

$$G(s) = \frac{k}{1 + \tau s} \tag{22}$$

In our case:

$$G(s) = \frac{1.5}{1 + 0.4s} \tag{23}$$

According to the structure shown in Fig. 7, the open-loop transfer function is:

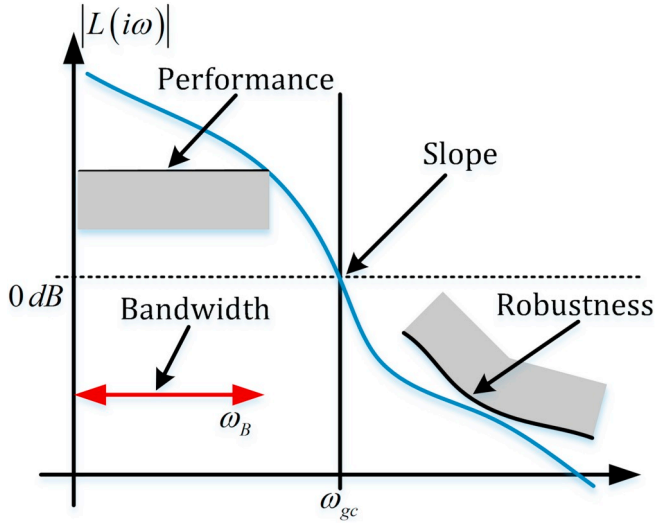

Fig. 6. Loop shaping behavior.

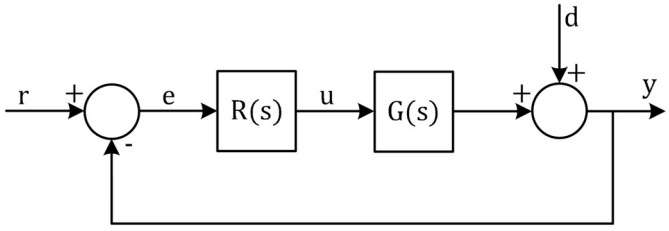

Fig. 7. Loop shaping block diagram.

$$L = G_{BO}(s) = R(s)\cdot G(s) \tag{24}$$

The bloc $R(s)$ represent the transfer function of the controller, which is used to force the output y (Fig. 7) to track the reference signal r and to reduce the effect of the perturbation signal d on the output y.

We use a proportional integral (PI) controller defined in (25) this controller has two free design parameters R_0 and ω_{gc}.

$$R(s) = R_0\left(1 + \frac{\omega_{g\,c}}{s}\right) \tag{25}$$

where

ω_{gc}: Pulsation to ensure high gain at low frequency.

The closed-loop transfer function is obtained as:

$$y = \frac{G(s)R(s)}{1 + G(s)R(s)}r + \frac{1}{1 + G(s)R(s)}d \tag{26}$$

$$y = \frac{L}{1 + L}r + \frac{1}{1 + L}d \tag{27}$$

where

$$L = G(s)R(s) = G_{BO}(s) \tag{28}$$

L is called the open-loop transfer function. It is worth noticing that in order to y track the reference r the gain of L must be large in the frequency rang where r is defined (the bandwidth).

If R(s) is chosen such that L is much larger than 1 ($L \gg 1$), the closed loop transfer function becomes:

$$y = r, \text{ with} \begin{cases} \frac{L}{1 + L} = 1 \\ \frac{1}{1 + L} = 0 \end{cases} \|L\| \gg 1 \tag{29}$$

The first term $\frac{L}{1+L}$ can be approximated to 1 and the second term $\frac{1}{1+L}$ can be approximated to 0 so the output $y = r$where

$$\begin{cases} k_p = R_0 = 0.05 \\ k_I = R_0\omega_{gc} = 5 \\ \omega_{gc} = 100rad/s \end{cases} \tag{30}$$

In addition, L must have small gain for high frequencies to guarantee robustness [34,35].

Using the same approach as above the designed PI controller for induction motor speed control loop is given by:

$$\begin{cases} k_p = R_0 = 0.2339 \\ k_I = R_0\omega_{gc} = 70.7887 \\ \omega_{gc} = 302.64rad/s \end{cases} \tag{31}$$

Loop 2: the Super-twisting algorithm is a second order sliding mode controller [36,37] applicable to systems with relative degree one. The latter is the number of time the derivative of the output signal we need before the input shows up. The advantage of this algorithm is that it does not require the time derivative information of the sliding variables [38] and reduce significantly the chattering phenomena inherent in first order sliding mode control [39,40]

This algorithm defines the control law as a combination of two terms, continuous sliding variable function, and the second term is the integral of a discontinuous function of the sliding variable [40,41].

Notice that we have chosen this algorithm since the relative degree of our system is [1,1] and this loop is inner loop with respect to loop 1. So it must be very fast which is an underlying property of sliding mode control (finite time convergence) [41].

The control law $U = [u_1 u_2]^T$ is designed to drive the system to the desired surface $S = [s_1 s_2]^T$ this latter is designed as:

$$S = \begin{bmatrix} s_1 \\ s_2 \end{bmatrix} = \begin{bmatrix} v_b - v_{b\,ref} \\ v_r - v_{r\,ref} \end{bmatrix} \tag{32}$$

where S is bypass stream and retentate stream velocities sliding surfaces respectively.

Proposition 1: Consider system (12) and the sliding surface S defined in (32). Let $U = U_{eq} + U_n$ With

$$U = \begin{bmatrix} u_1 \\ u_2 \end{bmatrix} = \begin{bmatrix} u_{1eq} + u_{1n} \\ u_{2eq} + u_{2n} \end{bmatrix} \tag{33}$$

where

U_n: is the switching control term. The switching control term make the system in any initial state reach the sliding manifold in finite time, which are calculated through application of the super-twisting algorithm.

U_{eq}: is the equivalent control term. The equivalent control term make the system move along the sliding manifold under ideal conditions, and these terms can speed up the response of the system and reduce the steady-state errors [40].

The equivalent control terms are calculated by setting $\dot{S} = 0$

$$\dot{S} = \begin{bmatrix} \dot{s}_1 \\ \dot{s}_2 \end{bmatrix} = \begin{bmatrix} \dot{v}_b - \dot{v}_{b\,ref} \\ \dot{v}_r - \dot{v}_{r\,ref} \end{bmatrix} = \begin{bmatrix} 0 \\ 0 \end{bmatrix} \tag{34}$$

$$U_{eq} = \begin{bmatrix} u_{1eq} \\ u_{2eq} \end{bmatrix} = \begin{bmatrix} \dfrac{\dot{v}_{b\,ref} \mathrm{V} - \frac{A_p^2}{A_m K_m}(v_f - v_b - v_r) - \frac{A_p}{\rho}\Delta\pi}{-0.5 A_p v_b^2} \\ \dfrac{\dot{v}_{r\,ref} \mathrm{V} - \frac{A_p^2}{A_m K_m}(v_f - v_b - v_r) - \frac{A_p}{\rho}\Delta\pi}{-0.5 A_p v_r^2} \end{bmatrix} \tag{35}$$

Using Eqs. (12), (33), (35)

$$U = \begin{bmatrix} \left(\dfrac{\dot{v}_{b\,ref} \mathrm{V} - \frac{A_p^2}{A_m K_m}(v_f - v_b - v_r) - \frac{A_p}{\rho}\Delta\pi}{-0.5 A_p v_b^2} \right) + \left(k_{11} \, |s_1|^{\frac{1}{2}} sign(s_1) + k_{12} \int sign(s_1) dt \right) \\ \left(\dfrac{\dot{v}_{r\,ref} \mathrm{V} - \frac{A_p^2}{A_m K_m}(v_f - v_b - v_r) - \frac{A_p}{\rho}\Delta\pi}{-0.5 A_p v_r^2} \right) + \left(k_{21} \, |s_2|^{\frac{1}{2}} sign(s_2) + k_{22} \int sign(s_2) dt \right) \end{bmatrix} \tag{36}$$

Then the tracking errors $e = \begin{bmatrix} e_1 \\ e_2 \end{bmatrix} = \begin{bmatrix} v_b - v_{b\,ref} \\ v_r - v_{r\,ref} \end{bmatrix}$ are globally asymptotically stable.

3.2. Stability proof

From equation

$$U = U_{eq} + U_n \tag{37}$$

In this case, the invariance condition is expressed as:

$$S = 0 \text{ and } \dot{S} = 0 \tag{38}$$

The dynamics of the system described by Eq. (17) is subjected to the following equation:

$$\dot{S} = \frac{\partial S}{\partial x}\frac{dx}{dt} \tag{39}$$

Since

$$\frac{dx}{dt} = \dot{x} = f(x) + g(x)U \tag{40}$$

And

$$U = U_{eq} + U_n \tag{41}$$

We have

$$\dot{S} = \frac{\partial S}{\partial x}[f(x) + g(x)U_{eq}] + \frac{\partial S}{\partial x}[g(x)U_n] \tag{42}$$

For $\dot{S} = 0$ and $U_n = 0$, we obtain

$$U_{eq} = -\left[\frac{\partial S}{\partial x} g(x)\right]^{-1}\left[\frac{\partial S}{\partial x} f(x)\right] \tag{43}$$

Using Eqs. (42), (43) we obtain

$$\dot{S} = \frac{\partial S}{\partial x} g(x) U_n \tag{44}$$

Let us choose the Lyapunov function such as

$$V = \frac{1}{2} S^T S \tag{45}$$

Its derivative is given by

$$\dot{V} = S^T \dot{S} = s_1 \dot{s}_1 + s_2 \dot{s}_2 \tag{46}$$

One must verify the decrease of the Lyapunov function to zero. For this purpose, it is sufficient to ensure that its derivative is negative definite.

$$\dot{V} < 0 \Rightarrow S^T \dot{S} < 0 \tag{47}$$

$$S^T \dot{S} = S^T \frac{\partial S}{\partial x} g(x) U_n = s_1^T \frac{\partial s_1}{\partial x_1} g_1(x) u_{1n} + s_2^T \frac{\partial s_2}{\partial x_2} g_2(x) u_{2n} < 0 \tag{48}$$

The form of the control action given by

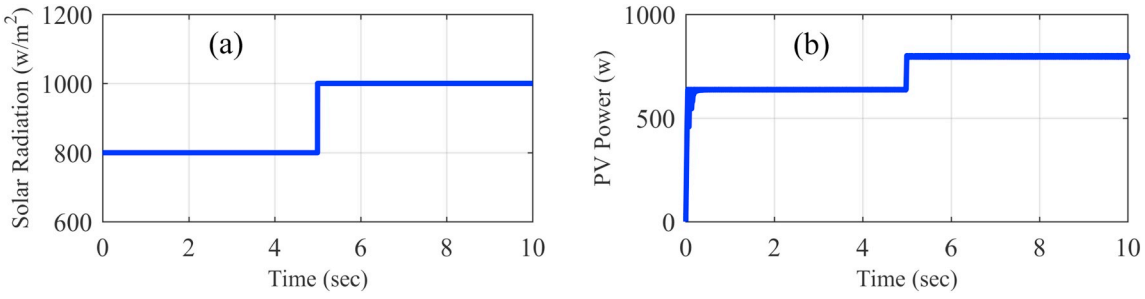

Fig. 8. (a) Profile of solar radiation. (b) Photovoltaic power output.

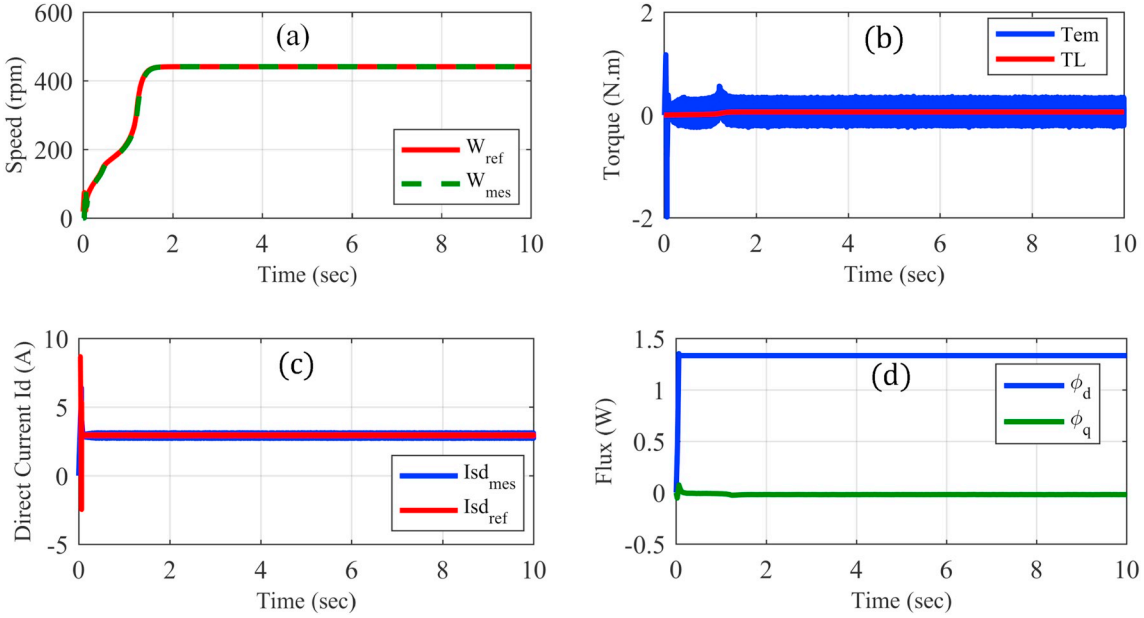

Fig. 9. (a) Profile of variable frequency drive speed (SVFD). (b) Resistive torque and electromagnetic torque responses. (c) Direct current response. (d) Rotor flux response.

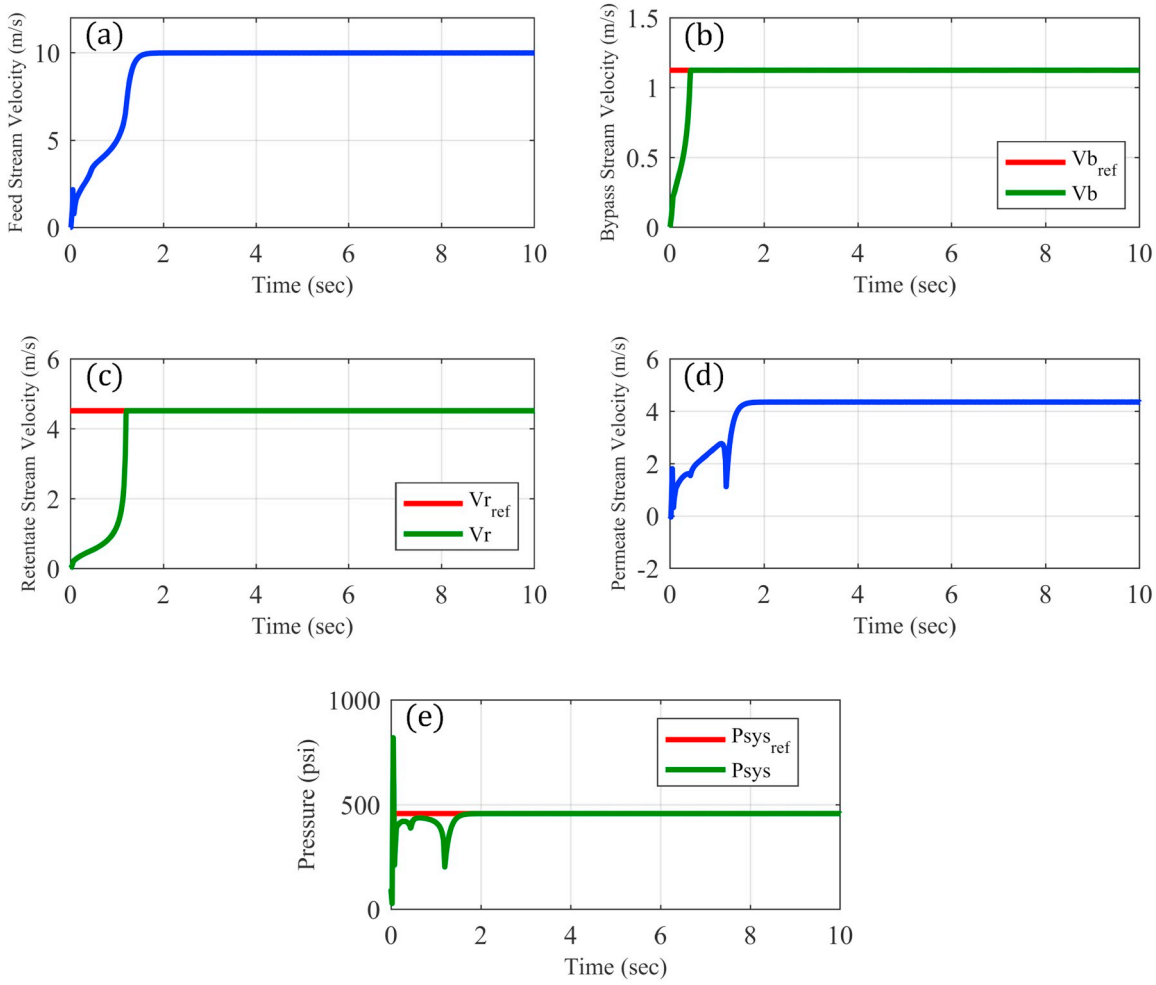

Fig. 10. (a) Profiles of feed stream velocity (vf). (b) Bypass stream velocity (vb). (c) Retentate stream velocity (vr). (d) Permeate stream velocity (vp). (e) System pressure (Psys).

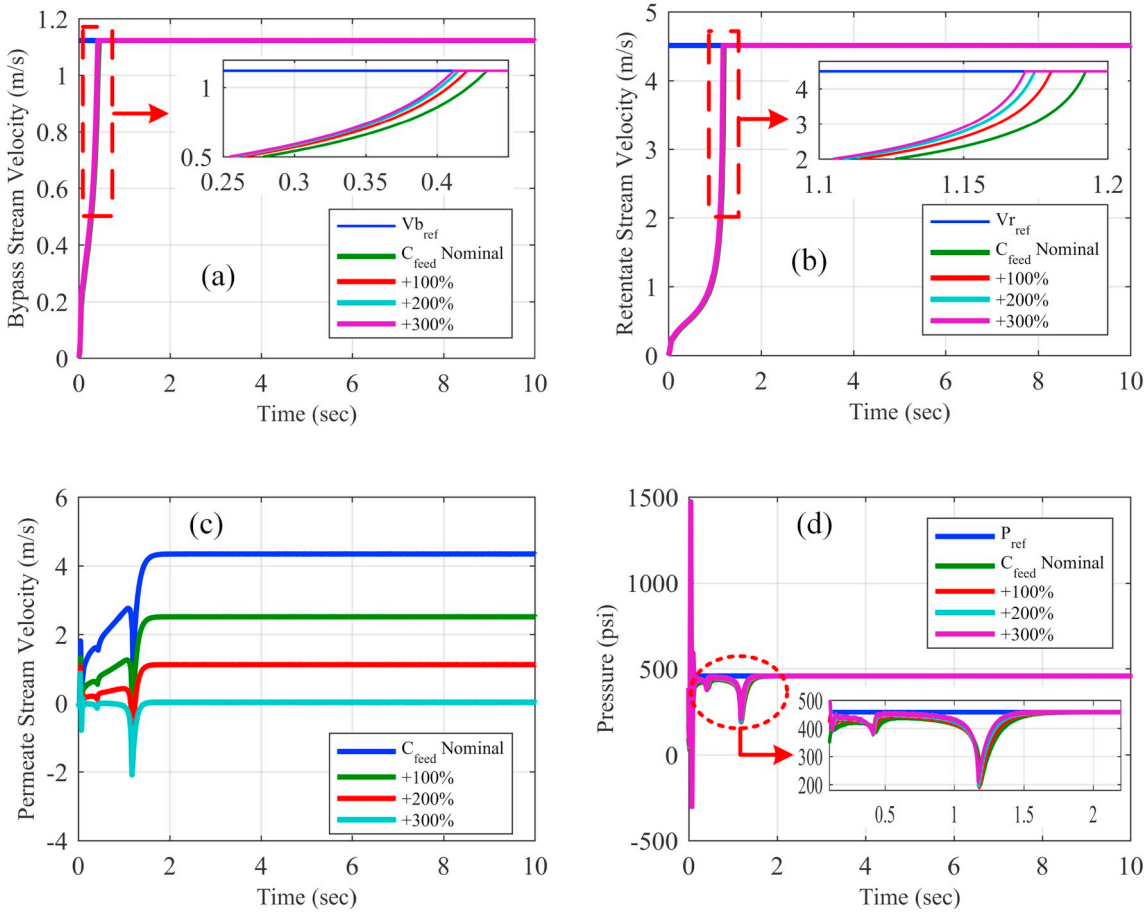

Fig. 11. Response results of RO system under feed salt concentration variation. (a) bypass stream velocity. (b) retentate stream velocity. (c) permeate stream velocity. (d) system pressure.

$$U_n = \begin{bmatrix} u_{1n} \\ u_{2n} \end{bmatrix} = \begin{bmatrix} k_{11}\ |s_1|^{\frac{1}{2}} sign(s_1) + k_{12} \int sign(s_1)dt \\ k_{21}\ |s_2|^{\frac{1}{2}} sign(s_2) + k_{22} \int sign(s_2)dt \end{bmatrix} \tag{49}$$

Replacing U_n in Eq. (48)

$$S^T\dot{S} = s_1 \frac{\partial s_1}{\partial x_1} g_1(x)\left(k_{11}\ |s_1|^{\frac{1}{2}} sign(s_1) + k_{12} \int sign(s_1)dt\right) + s_2 \frac{\partial s_2}{\partial x_2} g_2(x)\left(k_{21}\ |s_2|^{\frac{1}{2}} sign(s_2) + k_{22} \int sign(s_2)dt\right) < 0 \tag{50}$$

$$S^T\dot{S} = \frac{\partial s_1}{\partial x_1} g_1(x)\left(k_{11}\ |s_1|^{\frac{1}{2}} |s_1| + k_{12} s_1 \int sign(s_1)dt\right) + \frac{\partial s_2}{\partial x_2} g_2(x)\left(k_{21}\ |s_2|^{\frac{1}{2}} |s_2| + k_{22} s_2 \int sign(s_2)dt\right) < 0 \tag{51}$$

$$S^T\dot{S} = \begin{bmatrix} s_1\dot{s}_1 \\ s_2\dot{s}_2 \end{bmatrix} = \begin{bmatrix} -\frac{\partial s_1}{\partial x_1}\left(\frac{1}{2}\left(\frac{A_p v_b^2}{V}\right)\right)\left(k_{11}\ |s_1|^{\frac{1}{2}} |s_1| + k_{12} s_1 \int sign(s_1)dt\right) < 0 \\ -\frac{\partial s_2}{\partial x_2}\left(\frac{1}{2}\left(\frac{A_p v_r^2}{V}\right)\right)\left(k_{21}\ |s_2|^{\frac{1}{2}} |s_2| + k_{22} s_2 \int sign(s_2)dt\right) < 0 \end{bmatrix} \tag{52}$$

$$\frac{\partial s_1}{\partial x_1} = \frac{\partial s_2}{\partial x_2} = 1 \tag{53}$$

The term $\left(\frac{\partial S}{\partial x}\right)g(x)$ is negative definite for the class of systems considered, where the gains k_{11}, k_{12} and k_{21}, k_{22} is chosen positive to satisfy stability conditions.

4. Simulation results and discussion

In order to demonstrate the effectiveness of the proposed control technique applied to the RO desalination system, various simulation tests of the overall architecture under a specific condition are implemented in MATLAB/Simulink using the parameters shown in the Appendix A.

In the first step, we started with the simulation of the proposed design scheme, which is described by Fig. 1 in order to study the behavior of the RO process during the application of the super-twisting sliding mode control without any external disturbances.

As seen in Fig. 8(a) the simulation test carried out under changing weather conditions where the solar radiation is started with E = 800 W/m^2 and at time t = 5 s is increased to E = 1000 W/m^2 with a constant temperature T = 25 °C.

Fig. 8(b) shows the evolution of the power output of the photovoltaic generator, we note that the P&O algorithm is robust to the quick variation of solar radiation and converges rapidly to the maximum power point (MPP) in a very short time.

One sees clearly in Fig. 9(a) that the speed of the induction motor follows perfectly its reference that is imposed by the system pressure regulator (S_{VFD}) (Fig. 1) with a good dynamic which shows the efficiency of the speed control loop, which subsequently allows achieving the desired flow rate of the pump. The electromagnetic torque instantly falls to a constant value in steady state; it is equal to the pump torque (Fig. 9(b)).

The direct stator current follows its reference accurately through the

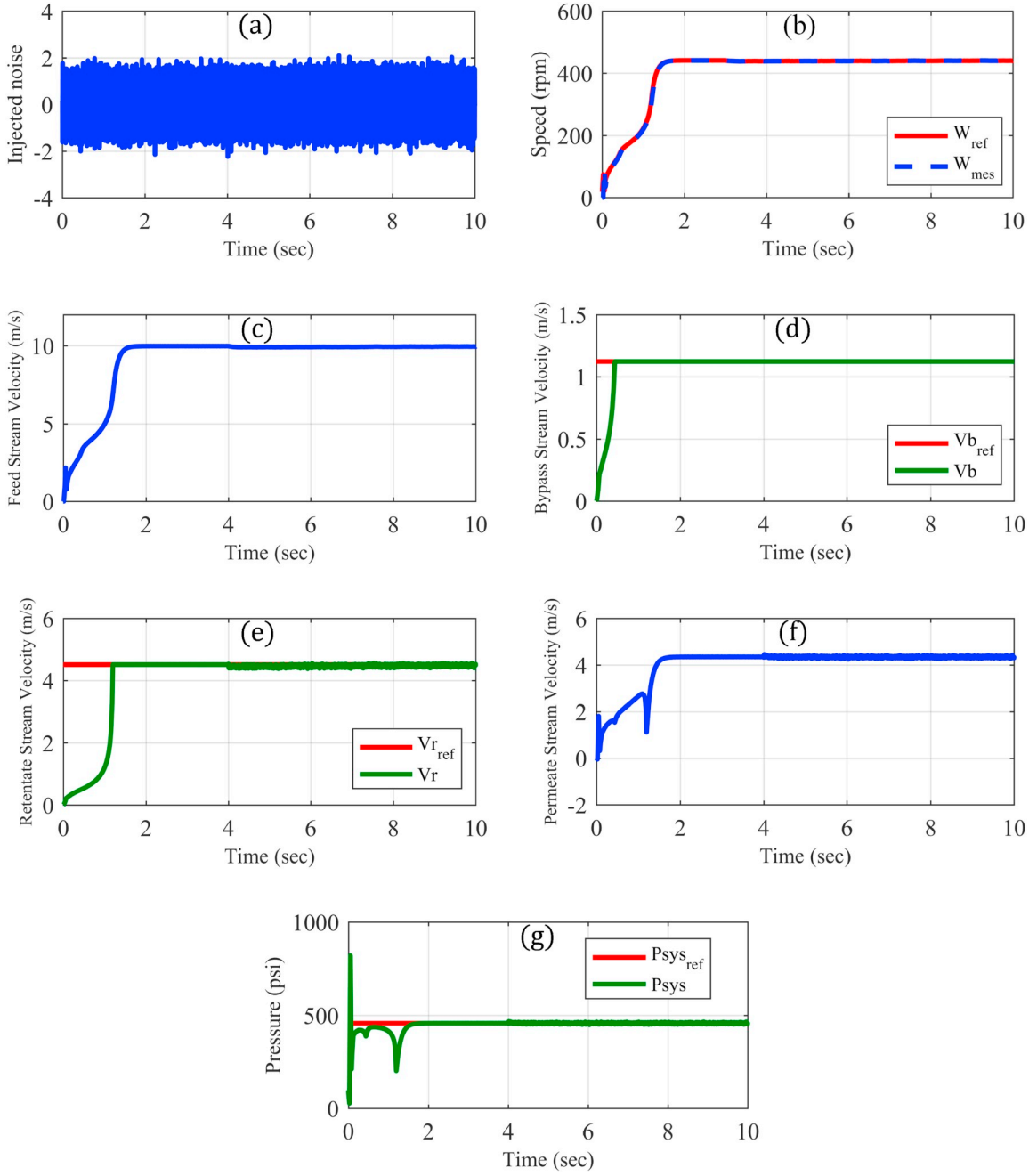

Fig. 12. Response results of RO system under noisy conditions. (a) Injected noise profile. (b) Variable frequency drive speed (SVFD). (c) Feed stream velocity. (d) Bypass stream velocity. (e) Retentate stream velocity. (f) Permeate stream velocity. (g) System pressure.

action of its PI controller (Fig. 9(c)). Fig. 9(d) shows the behavior of the direct and quadratic rotor flux. We notice that the quadratic flux is zero and the direct flux is constant which confirms that the decoupling is very well realized.

Robust PI controller is applied in the first loop to bring the system pressure to a set point of P_{sys} = 457.51 psi by adjusting the VFD speed which enables the control system to adjust the feed flow velocity. As seen in Fig. 10(a) the feed flow velocity is fixed at a constant value v_f = 10 m/s (desired value) in the input of the membrane because the pump reached its optimal speed (Fig. 9(a)). It can be noticed that the flow rate (flow velocity) of the pump depends on the induction motor speed.

The bypass flow velocity and retentate flow velocity were set to 1.123 m/s and 4.511 m/s respectively. Fig. 10(b) and (c) show the effectiveness of the proposed controller where the bypass flow velocity (v_b) and the retentate flow velocity (v_r) are fast enough to converge to its desired study state. It can be seen that the super-twisting sliding mode control achieves excellent tracking of the control variables with a small response time and there exist no overshoots.

Fig. 10(d) shows the behavior of the permeate stream velocity (v_p) at the outlet of the membrane. Controlling the permeate stream velocity depends on the control of the bypass stream velocity, retentate stream velocity, and the system pressure.

Fig. 10(e) shows that the system pressure at first deviates slightly to its desired value then reached its reference with good dynamics, which shows the efficiency of the robust PI regulator. It makes sense since the system pressure is the direct variable having an effect on the other variables. In fact, controlling the system pressure is the key in RO desalination performance.

The second set of simulation is designed to test the robustness of the

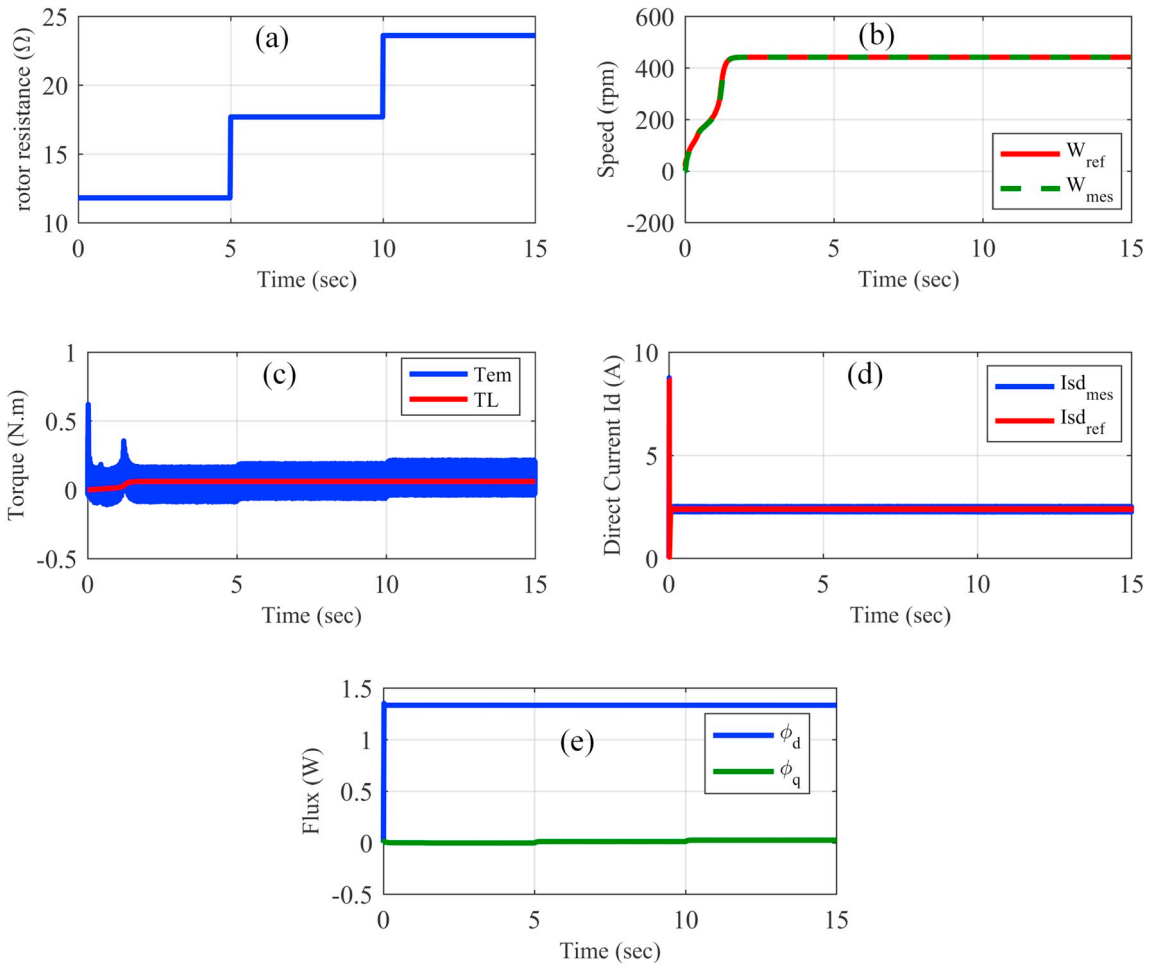

Fig. 13. (a) Profiles of rotor resistance variation. (b) variable frequency drive speed (SVFD). (c) Electromagnetic torque responses. (d) Direct current response. (e) Rotor flux response.

proposed controller when presented with a variation in feed water quality. It can be observed in Fig. 11(a) and (b) that the responses of the bypass stream velocity and retentate stream velocity converge fast enough to desired values and zero steady state errors during all the feed salt concentration changes. It can be clearly noticed that the super-twisting sliding mode controller can effectively cope with those parameter changes, with excellent performances.

As seen in Fig. 11(c) the permeate stream velocity decreases when the feed concentration increases, this result is expected because the increase in the feed concentration accompanied with an increase in the osmotic pressure leads to an increase of the resisting flow through the membrane.

The increase in osmotic pressure forces the system pressure to raise in order to keep the fixed feed rate. Therefore, the VFDs control must lower down the feed flow rate to maintain the system pressure at the set point of 457.51 psi as shown in Fig. 11(d)

In the real RO desalination plant operations, the measured outputs are subject to sensors measurement noises. In the third set of simulation, we introduce one noise signal at $t = 4$ s in the retentate flow sensor measurement to check the ability of the controller to effectively manipulate the system under noisy conditions. For this purpose, the additional white Gaussian measurement noise is shown in Fig. 12(a).

As shown in Fig. 12(e) we noticed that when we introduce the noise signal the super-twisting sliding mode controller rejects about 90% of sensor noise measurement and forces the measured variable state (retentate stream velocity) to match its reference at steady state. In addition, the bypass stream velocity will not be affected by the measurement noise uncertainty (Fig. 12(d)).

In Fig. 12(g) the system pressure is given under noisy measurement condition. One may easily notice that the system pressure remained stable and quite close to his reference; the measurement noise should be quickly dampened out with time (the VFD control loop is maintained at a pressure set point of 457.51 psi). The good behavior of the system pressure results in a smoothness of the pump speed response (there are no oscillations) (Fig. 12(b)) and, in turn, the feed flow velocity is maintained at constant value $v_f = 10$ m/s (Fig. 12(c)).

This result demonstrates the measurement noise immunity of the super-twisting sliding mode controller. Furthermore, it can eliminate measurement noise up to a certain limit; this means that in the case of large distortion caused by noise measurement the super-twisting sliding mode controller can provide safe operation for RO desalination process.

The complete architecture of RO desalination system powered by a photovoltaic source can suffer from various faults that can occur in any part thereof. For this reason, in this last part of the simulation, a fault tolerant control (FTC) test is carried out in order to check the ability of the controllers to deal with faulty conditions.

A rotor resistance variation is presented in this set of simulation to investigate the field oriented controller (FOC) performance under parameter changes along with an actuator fault in the RO membrane unite is introduced to teste the super-twisting sliding mode controller performance against faults.

As seen in Fig. 13(a) the rotor resistance is varying up to 50% at time $t = 5$ s, then to 100% at time $t = 10$ s of its nominal value.

Fig. 13(b) and (c) show that the speed tracks perfectly its reference with a good dynamics and the electromagnetic torque remains constant

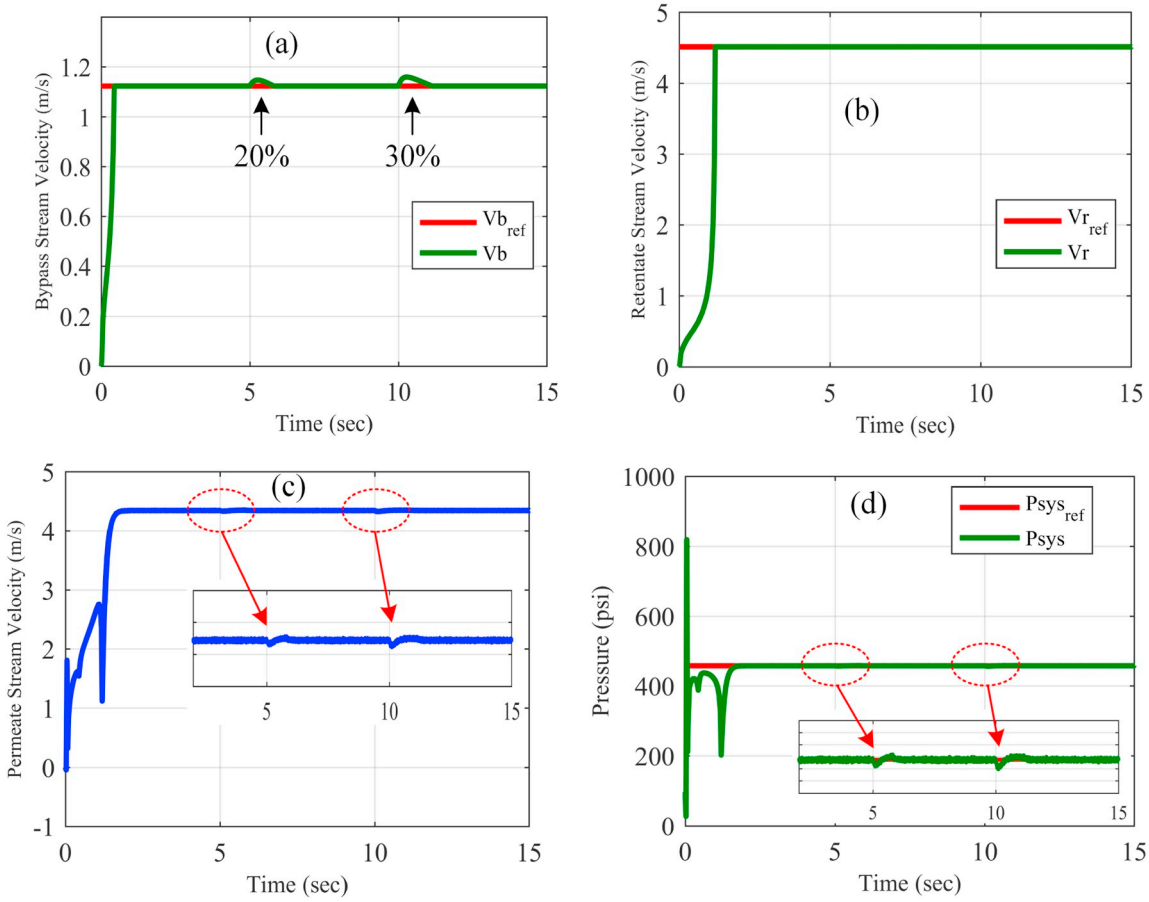

Fig. 14. Response results of RO system under faulty conditions (a) bypass stream velocity. (b) Retentate stream velocity. (c) Permeate stream velocity. (d) System pressure.

in spite of rotor resistance changes.

Fig. 13(d) shows that the direct stator current tracks the reference value adequately even with the changes in the rotor resistance value.

The behavior of the direct and quadratic rotor flux is shown in Fig. 13(e). It can be seen that even the increase in the rotor resistance value the direct rotor flux maintains its constant value equal to ϕ_r and the rotor quadratic flux remains zero.

We note that satisfactory performances are achieved under rotor resistance variation and the vector control has a good performance tracking.

The fault type is considered such as loss of effectiveness in the bypass valve of 20% at time t = 5 s and 30% at time t = 10 s.

Fig. 14(a) and (b) show the behavior of the bypass stream velocity and retentate stream velocity respectively under loss of effectiveness fault condition. When the fault occurs, the super-twisting sliding mode controller has attenuated the effect of fault after a few seconds of its occurrence and zero steady state error, which shows efficiency and robustness of the controller.

As seen in Fig. 14(d) the appearance of the fault induce a very smallest deviation from the system pressure set point that finds his reference quickly which leads the permeate stream velocity remained stable (Fig. 14(c)).

These results demonstrate that the proposed fault tolerant controller (FTC) using super-twisting sliding mode control is able to guarantee better tracking performances under nominal and faulty conditions.

5. Conclusion

In this paper, a new application of super-twisting sliding mode control has been proposed for the control of reverse-osmosis (RO) membrane water desalination system. This nonlinear controller was used to manipulate the bypass and retentate stream actuated valves, along with loop shaping PI controller that was used to manipulate the VFD speed, adjusting the feed flow rate. In addition, a complete reverse osmosis (RO) desalination chain was implemented in MATLAB/Simulink containing a photovoltaic power source, an induction motor associated with centrifugal pump and RO membrane unit. Each part of this architecture was presented with its own controller. The performance of the proposed control for the RO system is analyzed under several conditions such as nominal and with uncertainties caused by parametric variations or adding noise measurement and under faulty conditions which the improved control characteristics is achieved. Simulation results confirm the robustness and efficiency of the proposed scheme.

Nomenclature

RO	reverse osmosis
PVG	photovoltaic generator
FOC	field oriented control
MPPT	maximum power point tracking
P&O	perturb and observe
VFD	variable frequency drive
FTC	fault tolerant control
I_{pv}	photovoltaic currents of array
I_0	reverse saturation currents of diode
T_L	hydrodynamic load torque of the pump
Q	flow rate of the pump
H	total height of the pump
L_r	rotor phase inductance

L_s	stator phase inductance
L_m	magnetizing inductance
R_r	rotor phase resistance
R_s	stator phase resistance
p	pole pairs number
J	inertia moment
f	friction coefficient
ω_s	angular slip frequency
ω_r	angular rotor speed
v_{dq}	d and q axis component of stator voltage
Φdq	instantaneous values of the rotor flux (d, q) components
i_{dq}	instantaneous values of the stator currents (d, q) components
σ	leakage coefficient
v_b	bypass stream velocity
v_r	retentate stream velocity
v_f	feed stream velocity
v_p	permeate stream velocity
e_{vb}	bypass valve resistance
e_{vr}	retentate valve resistance
$\Delta\pi$	osmotic pressure
P_{sys}	system pressure

Appendix A

Table 1
System parameters.

PVG parameters	
I_{mp}	7.61 A
P_{max}	200.143 W
I_{sc}	8.21 A
V_{oc}	32.9 V
N_s	54
Np	4
Induction motor parameters	
P	750 W
Rs	11.3085 Ω
Rr	11.8 Ω
Ls	0.5578H
Lr	0.6152H
Lm	0.5578H
J	$0.0020\,kg \cdot m^2$
F	$3.1165 \cdot 10^{-4}$ Nm/rad/s
P	1
Centrifugal pump parameters	
Q_{max}	$30\,m^3/h$
H	80 m
N	2900 r/min
RO process parameters	
ρ	$1000\,kg/m^3$
V	$0.04\,m^3$
A_p	$1.27\,cm^2$
A_m	$30\,m^2$
K_m	$9.218 \cdot 10^{-9}$ s/m
α	0.5
T	25 °C
R	0.993
δ	0.2641

References

[1] S. Sobana and R. C. Panda, “Modeling and control of reverse osmosis desalination process using centralized and decentralized techniques,” Desalination, vol. 344, no. Supplement C, pp. 243–251, Jul. 2014.

[2] L.F. Greenlee, D.F. Lawler, B.D. Freeman, B. Marrot, P. Moulin, Reverse osmosis desalination: water sources, technology, and today's challenges, Water Res. 43 (9) (2009) 2317–2348 May.

[3] M.A. Eltawil, Z. Zhengming, L. Yuan, A review of renewable energy technologies integrated with desalination systems, Renew. Sust. Energ. Rev. 13 (9) (2009) 2245–2262 Dec.

[4] M. A. Alghoul et al., “Design and experimental performance of brackish water reverse osmosis desalination unit powered by 2 kW photovoltaic system,” Renew. Energy, vol. 93, no. Supplement C, pp. 101–114, Aug. 2016.

[5] T. Zhao, R. Niu, M. Su, and T. Anderson, “Steady state and dynamic modeling of RO desalination modules and system using EES,” in 2011 IEEE International Conference on Robotics and Automation, 2011, pp. 1–4.

[6] Y.-Y. Lu, Y.-D. Hu, X.-L. Zhang, L.-Y. Wu, Q.-Z. Liu, Optimum design of reverse osmosis system under different feed concentration and product specification, J. Membr. Sci. 287 (2) (2007) 219–229 Jan.

[7] H. Sharon and K. S. Reddy, “A review of solar energy driven desalination technologies,” Renew. Sust. Energ. Rev., vol. 41, no. Supplement C, pp. 1080–1118, Jan. 2015.

[8] A.M. Bilton, L.C. Kelley, S. Dubowsky, Photovoltaic reverse osmosis — feasibility and a pathway to develop technology, Desalin. Water Treat. 31 (1–3) (2011) 24–34 Jul.

[9] E. Tzen, R. Morris, Renewable energy sources for desalination, Sol. Energy 75 (5) (2003) 375–379 Nov.

[10] I. Alatiqi, H. Ettouney, H. El-Dessouky, Process control in water desalination industry: an overview, Desalination 126 (1) (1999) 15–32 Nov.

[11] I. M. Alatiqi, A. H. Ghabris, and S. Ebrahim, “System identification and control of reverse osmosis desalination,” Desalination, vol. 75, no. Supplement C, pp. 119–140, Jan. 1989.

[12] B. D. H. Phuc, S.-S. You, T.-W. Lim, and H.-S. Kim, “Dynamical analysis and control synthesis of RO desalination process against water hammering,” Desalination, vol. 402, no. Supplement C, pp. 133–142, Jan. 2017.

[13] C.W. McFall, A. Bartman, P.D. Christofides, Y. Cohen, Control and monitoring of a high recovery reverse osmosis desalination process, Ind. Eng. Chem. Res. 47 (17) (2008) 6698–6710 Sep.

[14] A.R. Bartman, P.D. Christofides, Y. Cohen, Nonlinear model-based control of an experimental reverse-osmosis water desalination system, Ind. Eng. Chem. Res. 48 (13) (2009) 6126–6136 Jul.

[15] M. Arrouf, S. Ghabrour, Modelling and simulation of a pumping system fed by photovoltaic generator within the Matlab/Simulink programming environment, Desalination 209 (1) (2007) 23–30. Apr.

[16] A.P.C.-E. Feraga, A. Bouldjedri, Performance of a photovoltaic pumping system driven by a single phase induction motor connected to a photovoltaic generator, Automatika 57 (1) (2016) 163–172 Jan.

[17] D.S.H. Chan, J.R. Phillips, J.C.H. Phang, A comparative study of extraction methods for solar cell model parameters, Solid State Electron. 29 (3) (1986) 329–337 Mar.

[18] K. Rahrah, D. Rekioua, T. Rekioua, S. Bacha, Photovoltaic pumping system in Bejaia

climate with battery storage, Int. J. Hydrog. Energy 40 (39) (2015) 13665–13675 Oct.
[19] M. G. Villalva, J. R. Gazoli, and E. R. Filho, "Modeling and circuit-based simulation of photovoltaic arrays," in 2009 Brazilian Power Electronics Conference, 2009, pp. 1244–1254.
[20] A. Pandey, N. Dasgupta, A.K. Mukerjee, High-performance algorithms for drift avoidance and fast tracking in solar MPPT system, IEEE Trans. Energy Convers. 23 (2) (2008) 681–689 Jun.
[21] R. John, S. S. Mohammed, and R. Zachariah, "Variable step size Perturb and observe MPPT algorithm for standalone solar photovoltaic system," in 2017 IEEE International Conference on Intelligent Techniques in Control, Optimization and Signal Processing (INCOS), 2017, pp. 1–6.
[22] J.P. Ram, T.S. Babu, N. Rajasekar, A comprehensive review on solar PV maximum power point tracking techniques, Renew. Sust. Energ. Rev. 67 (2017) 826–847 Jan.
[23] C. Serir, D. Rekioua, N. Mezzai, S. Bacha, Supervisor control and optimization of multi-sources pumping system with battery storage, Int. J. Hydrog. Energy 41 (45) (2016) 20974–20986 Dec.
[24] M.A. Abdullah, A.H.M. Yatim, C.W. Tan, R. Saidur, A review of maximum power point tracking algorithms for wind energy systems, Renew. Sust. Energ. Rev. 16 (5) (2012) 3220–3227 Jun.
[25] M. Ouada, M. S. Meridjet, M. S. Saoud, And N. Derradji, "Study of new configuration photovoltaic pumping system," in 2014 International Conference on Electrical Sciences and Technologies in Maghreb (CISTEM), 2014, pp. 1–5.
[26] H. Bouzeria, C. Fetha, T. Bahi, and L. Rachedi, "Speed control of induction motor-pump supplied by photovoltaic generator," in 3rd International Conference on Systems and Control, 2013, pp. 445–450.
[27] P.G. Kini, R.C. Bansal, R.S. Aithal, Performance analysis of centrifugal pumps subjected to voltage variation and unbalance, IEEE Trans. Ind. Electron. 55 (2) (2008) 562–569 Feb.
[28] P. Vas, Sensorless Vector and Direct Torque Control, OUP Oxford, Oxford; New York, 1998.
[29] S. G. Malla, C. N. Bhende, and S. Mishra, "Photovoltaic based water pumping system," in 2011 International Conference on Energy, Automation and Signal, 2011, pp. 1–4.
[30] M.A. Vitorino, M.B. de R. Correa, C.B. Jacobina, A.M.N. Lima, An effective induction motor control for photovoltaic pumping, IEEE Trans. Ind. Electron. 58 (4) (Apr. 2011) 1162–1170.
[31] A. Gouichiche, S. Boucherit, M. Tadjine, A. Safa, Y. Messlem, An improved stator winding fault tolerance architecture for vector control of induction motor: theory and experiment, Electr. Power Syst. Res. 104 (Nov. 2013) 129–137.
[32] A.R. Bartman, C.W. McFall, P.D. Christofides, Y. Cohen, Model-predictive control of feed flow reversal in a reverse osmosis desalination process, J. Process Control 19 (3) (2009) 433–442 Mar.
[33] A.R. Bartman, A. Zhu, P.D. Christofides, Y. Cohen, Minimizing energy consumption in reverse osmosis membrane desalination using optimization-based control, J. Process Control 20 (10) (2010) 1261–1269 Dec.
[34] A.T. Azar, S. Vaidyanathan, Advances in System Dynamics and Control, IGI Global, 2001.
[35] B.D.H. Phuc, S.-S. You, T.-W. Lim, H.-S. Kim, Modified PID control with H∞ loop shaping synthesis for RO desalination plants, Desalin. Water Treat. 57 (53) (2016) 25421–25434 Nov.
[36] W. Perruquetti, J.P. Barbot, Sliding Mode Control in Engineering, CRC Press Inc., New York, 2002.
[37] Y. Shtessel, C. Edwards, L. Fridman, A. Levant, Sliding Mode Control and Observation, Birkhäuser Basel, 2014.
[38] X. Zhu, S. Liu, and Y. Wang, "Second-order Sliding-mode Control of DFIG-based Wind Turbines," p. 8.51–8.51, Jan. 2014.
[39] A.K. Pati, N.C. Sahoo, Adaptive super-twisting sliding mode control for a three-phase single-stage grid-connected differential boost inverter based photovoltaic system, ISA Trans. 69 (2017) 296–306 Jul.
[40] M. Derbeli, M. Farhat, O. Barambones, L. Sbita, Control of PEM fuel cell power system using sliding mode and super-twisting algorithms, Int. J. Hydrog. Energy 42 (13) (2017) 8833–8844 Mar.
[41] C. Lascu and F. Blaabjerg, "Super-twisting sliding mode direct torque contol of induction machine drives," in 2014 IEEE Energy Conversion Congress and Exposition (ECCE), 2014, pp. 5116–5122.